

# D-Scan measurement of ablation threshold incubation effects for ultrashort laser pulses

Leandro Matioli Machado, Ricardo Elgul Samad,\* Wagner de Rossi, and Nilson Dias Vieira Junior

Centro de Lasers e Aplicações – IPEN-CNEN/SP – Av. Prof. Lineu Prestes 2242, 05508-000, São Paulo, Brazil  
\*resamad@gmail.com

**Abstract:** We report the validation of the Diagonal Scan (D-Scan) technique to determine the incubation parameter for ultrashort laser pulses ablation. A theory to calculate the laser pulses superposition and a procedure for quantifying incubation effects are described, and the results obtained for BK7 samples in the 100 fs regime are compared to the ones given by the traditional method, showing a good agreement.

©2012 Optical Society of America

**OCIS codes:** (320.2250) Femtosecond phenomena; (160.2750) Glass and other amorphous materials; (160.4670) Optical materials; (220.4610) Optical fabrication; (320.7130) Ultrafast processes in condensed matter, including semiconductors.

---

## References and links

1. N. Bloembergen, "Laser-induced electric breakdown in solids," *IEEE J. Quantum Electron.* **10**(3), 375–386 (1974).
2. D. Du, X. Liu, G. Korn, J. Squier, and G. Mourou, "Laser-induced breakdown by impact ionization in SiO<sub>2</sub> with pulse widths from 7 ns to 150 fs," *Appl. Phys. Lett.* **64**(23), 3071–3073 (1994).
3. J. Reif and F. Costache, "Femtosecond laser interaction with solid surfaces: explosive ablation and self-assembly of ordered nanostructures," in *Advances in Atomic Molecular, and Optical Physics*, V. 53, G. Rempe and M. O. Scully, eds. (Elsevier Academic Press Inc, 2006), pp. 227–251.
4. R. Stoian, A. Rosenfeld, D. Ashkenasi, I. V. Hertel, N. M. Bulgakova, and E. E. B. Campbell, "Surface charging and impulsive ion ejection during ultrashort pulsed laser ablation," *Phys. Rev. Lett.* **88**(9), 097603 (2002).
5. M. D. Perry, B. C. Stuart, P. S. Banks, M. D. Feit, V. Yanovsky, and A. M. Rubenchik, "Ultrashort-pulse laser machining of dielectric materials," *J. Appl. Phys.* **85**(9), 6803–6810 (1999).
6. W. Kautek, J. Kruger, M. Lenzner, S. Sartania, C. Spielmann, and F. Krausz, "Laser ablation of dielectrics with pulse durations between 20 fs and 3 ps," *Appl. Phys. Lett.* **69**(21), 3146–3148 (1996).
7. L. V. Keldysh, "Ionization in the field of a strong electromagnetic wave," *Sov. Phys. JETP-USSR* **20**, 1307–1314 (1965).
8. M. Lenzner, J. Kruger, S. Sartania, Z. Cheng, C. Spielmann, G. Mourou, W. Kautek, and F. Krausz, "Femtosecond optical breakdown in dielectrics," *Phys. Rev. Lett.* **80**(18), 4076–4079 (1998).
9. A. P. Joglekar, H. Liu, G. J. Spooner, E. Meyhofer, G. Mourou, and A. J. Hunt, "A study of the deterministic character of optical damage by femtosecond laser pulses and applications to nanomachining," *Appl. Phys. B* **77**, 25–30 (2003).
10. S. Nolte, C. Momma, H. Jacobs, A. Tunnermann, B. N. Chichkov, B. Wellegehausen, and H. Welling, "Ablation of metals by ultrashort laser pulses," *J. Opt. Soc. Am. B* **14**(10), 2716–2722 (1997).
11. E. G. Gamaly, A. V. Rode, B. Luther-Davies, and V. T. Tikhonchuk, "Ablation of solids by femtosecond lasers: ablation mechanism and ablation thresholds for metals and dielectrics," *Phys. Plasmas* **9**(3), 949–957 (2002).
12. F. Costache, S. Eckert, and J. Reif, "Near-damage threshold femtosecond laser irradiation of dielectric surfaces: desorbed ion kinetics and defect dynamics," *Appl. Phys., A Mater. Sci. Process.* **92**(4), 897–902 (2008).
13. M. Mero, B. Clapp, J. C. Jasapara, W. Rudolph, D. Ristau, K. Starke, J. Kruger, S. Martin, and W. Kautek, "On the damage behavior of dielectric films when illuminated with multiple femtosecond laser pulses," *Opt. Eng.* **44**(5), 051107 (2005).
14. L. C. Courrol, R. E. Samad, L. Gomez, I. M. Ranieri, S. L. Baldochi, A. Zanardi de Freitas, and N. D. Vieira, "Color center production by femtosecond pulse laser irradiation in LiF crystals," *Opt. Express* **12**(2), 288–293 (2004).
15. D. Ashkenasi, M. Lorenz, R. Stoian, and A. Rosenfeld, "Surface damage threshold and structuring of dielectrics using femtosecond laser pulses: the role of incubation," *Appl. Surf. Sci.* **150**(1-4), 101–106 (1999).
16. S. Martin, A. Hertwig, M. Lenzner, J. Kruger, and W. Kautek, "Spot-size dependence of the ablation threshold in dielectrics for femtosecond laser pulses," *Appl. Phys., A Mater. Sci. Process.* **77**, 883–884 (2003).
17. Y. Jee, M. F. Becker, and R. M. Walser, "Laser-induced damage on single-crystal metal surfaces," *J. Opt. Soc. Am. B* **5**(3), 648–659 (1988).

18. Y. C. Lim, P. E. Boukany, D. F. Farson, and L. J. Lee, "Direct-write femtosecond laser ablation and DNA combing and imprinting for fabrication of a micro/nanofluidic device on an ethylene glycol dimethacrylate polymer," *J. Micromech. Microeng.* **21**(1), 015012 (2011).
19. D. Gomez and I. Goenaga, "On the incubation effect on two thermoplastics when irradiated with ultrashort laser pulses: Broadening effects when machining microchannels," *Appl. Surf. Sci.* **253**(4), 2230–2236 (2006).
20. H. W. Choi, D. F. Farson, J. Bovatsek, A. Arai, and D. Ashkenasi, "Direct-write patterning of indium-tin-oxide film by high pulse repetition frequency femtosecond laser ablation," *Appl. Opt.* **46**(23), 5792–5799 (2007).
21. J. Bonse, J. M. Wrobel, J. Krüger, and W. Kautek, "Ultrashort-pulse laser ablation of indium phosphide in air," *Appl. Phys., A Mater. Sci. Process.* **72**(1), 89–94 (2001).
22. J. M. Liu, "Simple technique for measurements of pulsed Gaussian-beam spot sizes," *Opt. Lett.* **7**(5), 196–198 (1982).
23. R. E. Samad and N. D. Vieira, Jr., "Geometrical method for determining the surface damage threshold for femtosecond laser pulses," *Laser Phys.* **16**(2), 336–339 (2006).
24. R. E. Samad, S. L. Baldochi, and N. D. Vieira, Jr., "Diagonal scan measurement of Cr:LiSAF 20 ps ablation threshold," *Appl. Opt.* **47**(7), 920–924 (2008).
25. H. Kogelnik and T. Li, "Laser beams and resonators," *Appl. Opt.* **5**(10), 1550–1567 (1966).
26. M. Abramowitz and I. A. Stegun, *Handbook of mathematical functions with formulas, graphs, and mathematical tables*, 10th printing, with corrections. ed., United States National Bureau of Standards Applied mathematics series (U.S. Govt. Print. Off., 1972).
27. Wolfram Research Inc, "Jacobi theta function  $\theta_3$ " (1998–2011), retrieved 2011, <http://functions.wolfram.com/EllipticFunctions/EllipticTheta3/06/01/03/>.
28. A. Ben-Yakar and R. L. Byer, "Femtosecond laser ablation properties of borosilicate glass," *J. Appl. Phys.* **96**(9), 5316 (2004).
29. N. Sanner, O. Utéza, B. Bussiere, G. Coustillier, A. Leray, T. Itina, and M. Sentis, "Measurement of femtosecond laser-induced damage and ablation thresholds in dielectrics," *Appl. Phys., A Mater. Sci. Process.* **94**(4), 889–897 (2009).

## 1. Introduction

The ablation of solids by ultrashort laser pulses occurs after seed electrons are accelerated by the pulse electrical field, and either generate free electrons by collisions in an exponential avalanche process [1, 2], or are ejected from the surface due to the acquired kinetic energy [3]. The avalanche process results in a structural breakdown when the free electrons density reaches a critical value and transfers energy to lattice ions, which expand away from the surface after the pulse. The ions ejection is also assisted by a Coulomb explosion resulting from the charge deficiency originated by the surface ejected electrons [3, 4]. The seed electrons have different origins in diverse material classes: in metals, they are the conduction band free electrons, and in dielectrics and semiconductors they are excited from the valence to the conduction band by the pulse leading edge, either by multiphoton ionization [5, 6] or by tunneling induced by the laser field [7, 8]. Once free electrons are present, a metallization occurs in semiconductors and dielectrics, and the avalanche progresses deterministically in time [2, 9] in the same way in all materials [10, 11]. Due to these mechanisms, the ablation by ultrashort pulses has a nonselective character, and the only parameter that has to be known to etch a material is its ablation threshold fluence,  $F_{th}$ .

In a given material, the ablation threshold value can depend on the presence of impurities, defects, excitons, etc [12, 13], which either create intermediate levels in the bandgap or modify the local electronic density. As a consequence, seed electrons are created and ejected more easily than in the ideal material, and the avalanche happens at lower  $F_{th}$  values. The defects can be intrinsic to the material, or can be externally originated, such as laser created color centers [14]. In this case, when processing solids with superimposing pulses, modifications can be induced in the material, which will lower the  $F_{th}$  for subsequent pulses. These cumulative phenomena fall under the classification of incubation effects [15–17], and the ablation threshold fluence modifications induced by them must be taken into account when machining a material.

To quantify the incubation effects influence on the ablation threshold, its value is measured for various pulse superpositions, and then a function is fitted to the experimental data. One such function that allows the calculation of the incubation parameter  $S$  is [17]:

$$F_{th,N} = F_{th,1} N^{S-1}, \quad (1)$$

where  $F_{th,1}$  and  $F_{th,N}$  are the ablation threshold fluences for a single pulse and for the superposition of  $N$  pulses, respectively. Equation (1) arises from a simple probabilistic model [17], and was chosen here to obtain the incubation parameter due to its simplicity and use for various materials classes [17–20]. Although simple, this model characterizes the material response for cumulative ablation: for  $S < 1$ , incubation effects are present; if  $S = 1$ , the ablation threshold does not depend on the pulses superposition, and for  $S > 1$ , the material becomes more resistant to ablation as the pulses etch it (laser conditioning) [21]. Other models can be used to describe the incubation mechanisms [12–14], among which is the exponential defects accumulation model [12, 15], which considers a saturation of the defects accumulation that leads to a constant value of the ablation threshold fluence for the superposition of many pulses.

As for determining the  $F_{th}$  value for many pulses, the established procedure consists in applying the “zero damage method” [22] for various pulse superpositions, including the single pulse case. In this method, the surface of the sample is ablated at various fluences by a TEM<sub>00</sub> Gaussian beam, in different spots, and an exponential fit is performed to the data of the squared ablated diameter as a function of the pulse fluence. For this, the beam propagation must be known to estimate the beam size at the sample surface, and many measurements of the damage diameter must be done, originating large uncertainties for fluences close to the threshold, at which the damage size is close to zero and is difficult to be determined.

In the present work we use the diagonal scan (D-Scan) method introduced by us [23, 24], and extend its formalism to describe the measurement of the ablation threshold for the superposition of an arbitrary number of pulses. This allows the quantification of the incubation effects and the determination the incubation parameter for the sample under study. To validate the method, the ablation threshold and incubation parameter were determined in the 100 fs regime for Schott BK7 borosilicate glass, and its values were compared to the ones provided by the traditional method.

## 2. Theory

The D-Scan method for determining the ablation threshold fluence consists in moving the sample under study diagonally across the beamwaist of a focused laser beam [23, 24], etching the profile shown in Fig. 1 on its surface. It can be shown [23] that the ablation threshold fluence is given by:

$$F_{th} = \frac{E_0}{e\pi\rho_{\max}^2} \cong 0.117 \frac{E_0}{\rho_{\max}^2}, \quad (2)$$

where  $E_0$  is the pulse energy and  $\rho_{\max}$  is half of the ablation profile maximum transversal dimension. This maximum is located at the positions  $\pm\chi$  relative to the beamwaist, with  $\chi$  being given by [23]:

$$\chi = z_0 \sqrt{\frac{2}{e\pi w_0^2} \frac{E_0}{F_{th}} - 1}, \quad (3)$$

where  $w_0$  and  $z_0$  are the laser beam beamwaist and confocal parameter [25], respectively.

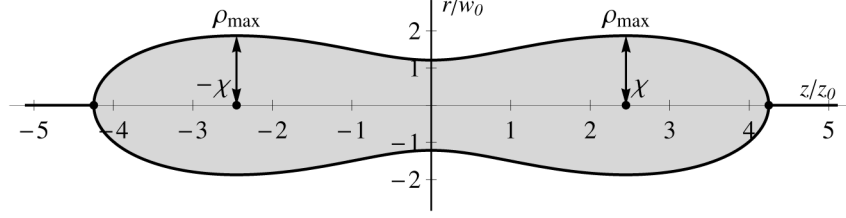


Fig. 1. Profile etched on the surface of a sample by the D-Scan method for  $P = 7P_{crit} = 7\frac{1}{2}e\pi w_0^2 I_{th}$  [23]. The axes are normalized by the beamwaist ( $w_0$ ) and the confocal parameter ( $z_0$ ), and the z-axis origin is at the beamwaist position.

From Eq. (2) it can be seen that the measurement of the ablation profile maximum transversal dimension and the pulse energy immediately determine the ablation threshold fluence,  $F_{th}$ .

To determine the ablation threshold fluence for many pulses,  $F_{th,N}$ , the pulses superposition that etches  $\rho_{max}$  at the  $\chi$  locus must be known. We hypothesize here that this superposition  $N$  at  $\chi$  is given by the sum of the intensities generated at this spot by all the pulses that hit the sample during a D-Scan, normalized by the intensity generated by the pulse centered at  $\chi$ . Then, to determine  $N$ , we initially calculate the intensity generated at the position  $(q, \chi)$  by a single pulse impinging on the sample at the position  $(0, y)$ , as indicated in Fig. 2. In this Fig., the y axis lies on the sample surface, and the z axis, which is the laser beam longitudinal axis, is transversal to the sample surface. The distance  $q$  from the y axis is used for generality.

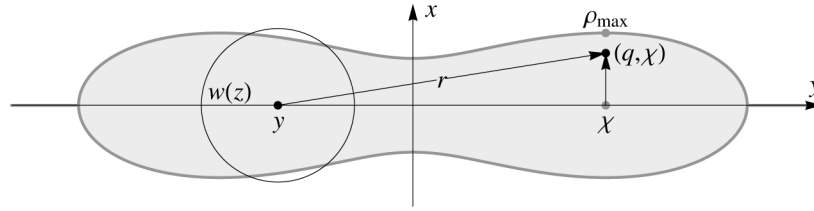


Fig. 2. Coordinates for the superposition derivation.

A pulse that hits the sample at  $(0, y)$  has a spot size  $w(z)$ , as shown in Fig. 2, and an intensity distribution given by [23]:

$$I(r, z) = \frac{2P_0}{\pi w(z)^2} e^{-2\frac{r^2}{w(z)^2}}, \quad (4)$$

where  $P_0$  is the pulse power,  $r$  is the radial distance and  $w(z)$  is given by the usual Gaussian propagation law [25]:

$$w(z) = w_0 \left[ 1 + \left( \frac{z}{z_0} \right)^2 \right]^{1/2}. \quad (5)$$

The intensity created by the pulse at  $(q, \chi)$  is then:

$$I(q, y, z) = \frac{2P_0}{\pi w(z)^2} e^{-2\frac{q^2 + (z-y)^2}{w(z)^2}}. \quad (6)$$

Now consider that at the time  $t_0=0$  a pulse hits the sample at  $y = \chi$ , generating the intensity  $I(q, \chi, z)$ . At this position, the beam generates the profile maximum,  $\rho_{max}$ , and by definition [23], the sample is located at  $z = \chi$  in the longitudinal axis; consequently, its intensity at  $(q, \chi)$  is  $I(q, \chi, \chi)$ . The next pulse will hit the sample after a time  $1/f$ , where  $f$  is the pulses repetition rate; after this interval, the sample has been displaced by  $v_y/f$  and  $v_z/f$  in the y and z directions,

where  $v_y$  and  $v_z$  are the displacement speeds in these directions, respectively [24]. Therefore, the intensity generated at  $(q, \chi)$  by the  $n^{\text{th}}$  pulse to hit the sample is  $I_{t_0+\frac{n}{f}} = I(q, \chi + n\frac{v_y}{f}, \chi + n\frac{v_z}{f})$ , given by:

$$I_{t_0+\frac{n}{f}} = \frac{2P_0}{\pi w(\chi + \frac{nv_z}{f})^2} e^{-\frac{q^2 + (\frac{nv_y}{f})^2}{w(\chi + \frac{nv_z}{f})^2}}, \quad (7)$$

and the total accumulated intensity at  $(q, \chi)$ ,  $I_{Tot}$ , is the summation of the contribution of all pulses that hit the sample:

$$I_{Tot} = \sum_{n=-\infty}^{\infty} I_{t_0+\frac{n}{f}} = \frac{2P_0}{\pi} \sum_{n=-\infty}^{\infty} \frac{1}{w(\chi + \frac{nv_z}{f})^2} e^{-\frac{q^2 + (\frac{nv_y}{f})^2}{w(\chi + \frac{nv_z}{f})^2}}. \quad (8)$$

To solve the sum shown in Eq. (8), let us consider that the beam spot size  $w(\chi + nv_z/f)$  does not change significantly around  $\chi$ , and can be considered to be constant and equal to  $w(\chi)$ , which is the spot size at  $t=t_0$ . This approximation considers that the transversal ( $v_y$ ) and longitudinal ( $v_z$ ) sample displacement speeds and the focusing lens should be chosen to produce an elongated ablation profile. Also, the approximation takes into account that the pulses, which have a spatial Gaussian intensity profile, contribute negligibly to the intensity at  $(q, \chi)$  when distant from  $\chi$  by a few spot sizes. Along with these considerations and the substitution of Eq. (3) in Eq. (5), which leads to  $w(\chi) = \sqrt{2}\rho_{\max}$ , Eq. (8) is rewritten to:

$$I_{Tot} = \frac{P_0}{\pi\rho_{\max}^2} e^{-\frac{q^2}{\rho_{\max}^2}} \sum_{n=-\infty}^{\infty} e^{-\left(\frac{v_y}{f\rho_{\max}}\right)^2 n^2}. \quad (9)$$

To obtain the pulse superposition  $N$ , Eq. (9) has now to be normalized by the intensity  $I_0$  of a single pulse centered at  $\chi$ . Substituting  $n = 0$  in Eq. (7) provides  $I_0$ , which is the term on the left of the summation symbol in Eq. (9), and consequently, the ratio  $N = I_{Tot}/I_0$  is simply:

$$N = \frac{I_{Tot}}{I_0} = \sum_{n=-\infty}^{\infty} e^{-\left(\frac{v_y}{f\rho_{\max}}\right)^2 n^2}. \quad (10)$$

The summation in Eq. (10) is one of the definitions of the Jacobi theta function  $\mathfrak{G}_3$  [26, 27], allowing it to be rewritten as:

$$N = \mathfrak{G}_3(0, e^{-\left(\frac{v_y}{f\rho_{\max}}\right)^2}), \quad (11)$$

providing a simple and analytical expression for the pulses superposition  $N$ .

Since  $v_y/(f\rho_{\max})$  is always positive, the second argument of the Jacobi theta function on Eq. (11) can only assume values between 0 and 1, limiting the range of  $N$  from 1 to infinity [26, 27], as expected. For high repetition rates or small displacement speeds, when the superposition of many pulses occur,  $v_y/(f\rho_{\max}) \approx 0$  and the second argument of  $\mathfrak{G}_3$  approaches the unity; in this limit the Jacobi theta function for real arguments can be approximated by:

$$\mathfrak{G}_3(0, x) \cong \sqrt{\frac{\pi}{1-x}}, \quad \text{for } x < 1. \quad (12)$$

Applying the identity shown in Eq. (12) to Eq. (11), and using the exponential function Taylor series expansion  $\text{Exp}\{-x^2\} \cong 1-x^2$  for  $x \approx 0$  in the result, leads to:

$$N = \sqrt{\pi} \frac{f \rho_{\max}}{v_y} \approx 1.8 \frac{f \rho_{\max}}{v_y}, \quad \text{for } \frac{v_y}{f \rho_{\max}} \approx 0, \quad (13)$$

providing a simple formula to determine the pulses superposition at the position  $\chi$  from the experimental data. For high transversal translation speeds or small repetition rates,  $v_y/(f \rho_{\max})$  tends to infinity, invalidating the approximation shown in Eq. (12), and consequently, Eq. (13) cannot be used; in this case Eq. (11) must be used, providing  $N$  values close to 1, as expected for the superposition of few pulses. Figure 3 shows a comparison between the superposition values calculated by the Jacobi theta Function (Eq. (11), red thick line) and the approximation for the superposition of many pulses (Eq. (13), black dashed line). It can be seen that the approximate solution, Eq. (13), departs from the analytical one, Eq. (11), only for  $v_y/(f \rho_{\max}) > 1$ , differing by less than 2.5% for values of this argument below 1.5. As a rule of thumb, Eq. (13) should be used to calculate  $N$  from the experimental parameters ( $v_y$ ,  $f$  and  $\rho_{\max}$ ) due to its simplicity; nevertheless, when this Eq. returns values smaller than 2, the Jacobi theta function, Eq. (11), must be used to provide the correct value of the superposition.

To ascertain the validity of the approximation that considers the beam spot size to be constant in the vicinity of  $\chi$ , Eq. (10) was calculated numerically for the case in which the summation index  $n$  is limited to the finite range from  $-m$  to  $+m$ . This represents the superposition of  $2m + 1$  pulses, and the results for  $m = 1, 10, 100$  and  $1000$  are shown in Fig. 3 as blue lines. It can be seen that the finite summation only diverges from the  $\mathcal{G}_3$  function (summation from  $-\infty$  to  $+\infty$ , red line in the graph) when the superposition  $N$  is larger than  $m$ . This means that only  $2m + 1 \approx 2N$  pulses have to be considered to obtain the superposition of  $N$  pulses at  $(q, \chi)$ ; once the experimental conditions (beam focusing and displacement speeds) for generating an elongated profile are satisfied, these  $2N$  pulses are in the immediate vicinity of  $\chi$ , and the more distant pulses do not contribute for the incubation effects at this position, as assumed by us when deriving Eq. (9). This validates our approximation.

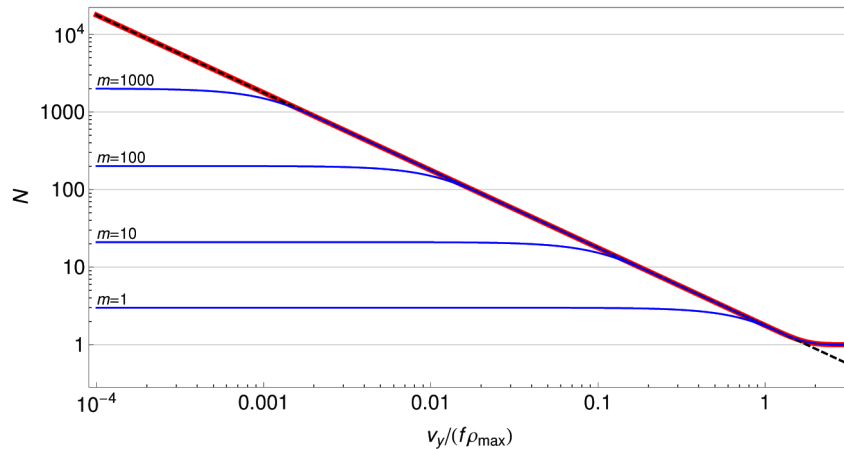


Fig. 3. Convergence of the approximations. The red line represents the analytical Jacobi theta function  $\mathcal{G}_3(0, \text{Exp}\{-[v_y / (f \rho_{\max})]^2\})$ , and the dashed line is the approximation for small values of the argument (Eq. (13)). The blue lines are the values of the finite summation for  $(2m + 1)$  terms, showing a divergence for  $N > m$ .

The superposition  $N$  defined here by Eq. (11) is not the same as the one used in the traditional method, in which the  $N$  pulses completely overlap. Nevertheless, we assume that these superpositions are equivalent once the numerical result of considering a finite number of terms on Eq. (10) demonstrates that only the pulses on the immediate vicinity of  $\chi$  contribute to the D-Scan superposition, in a condition that is similar to the traditional superposition.

Additionally, the present definition numerically allows fractionary superpositions, meaning that pulses whose spot size does not encompass the  $\rho_{max}$  position have a contribution that adds linearly to the incubation effects at this point.

Using the previous hypothesis and results, the determination of the ablation threshold fluence only requires performing a D-Scan on the sample, then the measurement of the etched profile maximum transversal dimension ( $2 \rho_{max}$ ); the use of the experimental values of  $v_y$ ,  $f$  and  $\rho_{max}$  in expressions (2) and (11) or (13) provides the  $F_{th}$  value for  $N$  pulses superposition, quantifying the incubation effects for this experimental condition.

### 3. Results

To validate the proposed method for the ablation threshold and incubation parameter determination, a CPA Ti:Sapphire laser system (Femtopower Compact Pro CE-Phase HP/HR from Femtolasers) was used, continuously generating 100 fs (FWHM) pulses centered at 775 nm with 40 nm of bandwidth (FWHM), at a maximum repetition rate of 4 kHz; the pulses were used to measure  $F_{th}$  and  $S$  in BK7 samples by the traditional and by the D-Scan methods, and the results were compared. All irradiations were done in air, and after etching the samples were cleaned with isopropyl alcohol in an ultrasonic cleaner to remove redeposited ablation debris. After cleaning, the samples were observed and photographed on an optical microscope, and the ablation dimensions were measured in the micrographs.

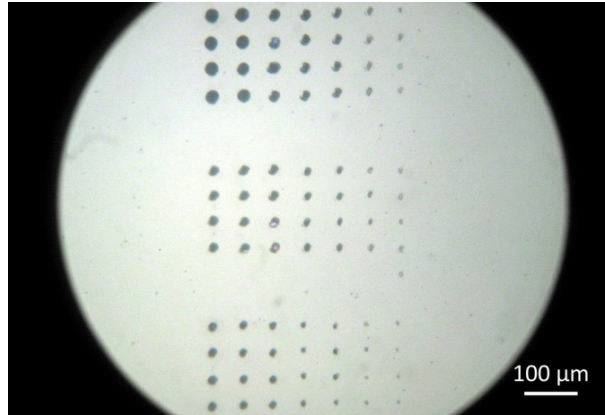


Fig. 4. Ablation spots on BK7 produced by the “zero damage method”.

For the “zero damage method”, the beam was focused by a 38 mm focal distance lens, and the samples were irradiated at various positions, with different energies and pulse superpositions. The micrograph shown in Fig. 4 depicts a sample in which ablation spots can be seen. Each vertical line shows the region ablated by the superposition of 2, 4, 16, 32, 120, 510, and 1020 pulses (from right to left), and each group of four horizontal lines (replicas) was etched with the same energy; each four lines group was machined with a different pulse energy, which for this sample were 2.9, 5, 7, 8.5, 12, 14 and 18.5  $\mu\text{J}$  (Fig. 4 shows the 12, 8.5 and 7  $\mu\text{J}$  results, from top to bottom). The ablated spots are separated by 60  $\mu\text{m}$  in the horizontal and 50  $\mu\text{m}$  in the vertical directions, and these distances were used as a scale to measure the regions diameters by software (ImageJ). The blurred region that is observed around each ablated spot was considered to be the uncertainty of the measured diameter. Two samples were etched, and the results averaged for each superposition. The ablation threshold fluences obtained are shown as red circles in Fig. 5.

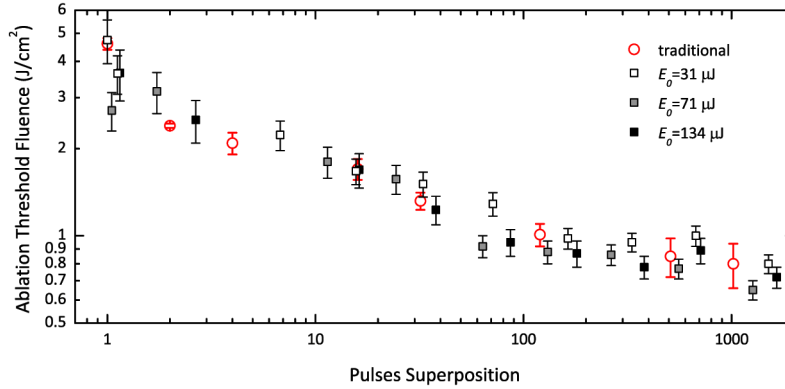


Fig. 5. Ablation threshold fluence dependence on the pulses superposition obtained by the “zero damage method” (red circles) and by the D-Scan method at three different energies (squares). The main contribution to the error bars came from the uncertainty of the ablated regions dimensions measurements.

For the D-Scan measurements, the laser was focused by the same 38 mm lens, and the BK7 samples were fixed, with their faces perpendicular to the laser beam, to a computer controlled translation table with 3 independent axes. The samples were irradiated by 31, 71 and 134  $\mu\text{J}$  pulses, and several superpositions were used for each pulse energy. To obtain the different superposition conditions, various laser repetition rates (50, 100, 500, 1000, 2000 and 4000 Hz) and constant sample transversal displacement speeds  $v_y$  [24] (6, 12, 25, 50 and 100 mm/min) were used; the transversal ( $v_y$ ) and longitudinal ( $v_z$ ) displacements speeds, were chosen in order to produce elongated etched profiles as shown in Fig. 6, satisfying the approximations that lead to Eq. (9). Also, the ratio  $v_y/v_z$  was kept constant between scans to produce profiles with the same length. Some combinations of  $f$  and  $v_y$  resulted in fractional superpositions. For each condition of energy and superposition, two scans were done and the etched profiles maximum transversal dimension were measured in the micrographs. Although the theory predicts that the etched profile must be symmetrical [23], asymmetries can be clearly seen in Fig. 6. This occurred because the left lobe of the profile was etched when the sample was located before the beam waist position, where a plasma is formed in the air. This plasma distorts the beam wavefront, modifying the beam, resulting in the etched profiles asymmetry. For this reason, the  $\rho_{max}$  was always measured on the left lobe, and the ablation threshold fluence values,  $F_{th}$ , were calculated using Eq. (2). As in the traditional method, the blur around each ablated region was considered to be the uncertainty of  $\rho_{max}$ , and the final  $\rho_{max}$  value is the average of the two measurements. Figure 6 shows two micrographs of the ablation profiles obtained for different superpositions, in which the measurements were taken. The software Mathematica was used to calculate all the superposition values ( $N$ ) using the Jacobi theta function, Eq. (11). The ablation threshold results obtained by the D-Scan method for each energy are shown in Fig. 5 as squares. In this Fig. is possible to see that the ablation threshold values obtained by the traditional and by the D-Scan methods show a good agreement, all dropping by factor close to 7 when going from a single pulse to the superposition of more than 1500 pulses. This graph demonstrates that the superposition defined in this work is equivalent to the traditional one in which the pulses overlap completely.

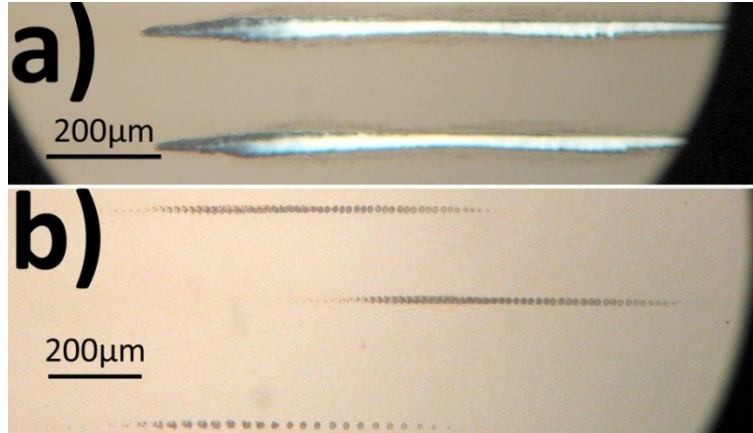


Fig. 6. Micrographs of samples etched by the D-Scan method. a) 1267.3 pulses superposition for  $E_0 = 71 \mu\text{J}$ , with a vertical separation of  $200 \mu\text{m}$  that was used as scale. b) for  $E_0 = 31 \mu\text{J}$ , the upper profiles, vertically separated by  $200 \mu\text{m}$ , represent 1.12 pulses superposition, and the lower profile is for a single pulse. The samples were cleaned in an ultrasonic cleaner with isopropyl alcohol.

To obtain the ablation threshold fluence for single pulses and the incubation parameter for each measurement series, Eq. (1) was fitted to each data set, and the parameters obtained are shown on Table 1. In this table, it can be seen that the values obtained for the single pulse ablation threshold fluence,  $F_{th,1}$ , are in agreement for all measurements, being consistent with the ones reported in the literature [28, 29]. Moreover, the agreement is better for the incubation parameter measured, considering the uncertainties. It should be noted that the uncertainties obtained by the D-Scan are smaller than by the traditional method, and this is a consequence of the dimensional measurements being always done in a region in which the relative uncertainty ( $\sigma_{\rho_{\max}}/\rho_{\max}$ ) is small. Computing the average weighed by the squared variances (ponderate mean) for each parameter obtained by the D-Scan method gives  $F_{th,1} = (3.29 \pm 0.16) \text{ J/cm}^2$  and  $S = (0.76 \pm 0.01)$ . These values are in excellent agreement with the ones obtained by the traditional method, validating the D-Scan as a method to measure incubation effects. Also, they demonstrate that incubation effects play an important role in the ablation of BK7 by ultrashort pulses, making the material easier to be processed as the pulses superposition increases.

Table 1. Fit Parameters Obtained by Both Methods

Method	$F_{th,1}$ ( $\text{J/cm}^2$ )	$S$
Traditional	$3.26 \pm 0.35$	$0.74 \pm 0.06$
D-Scan, 134 $\mu\text{J}$	$3.26 \pm 0.31$	$0.76 \pm 0.02$
D-Scan, 71 $\mu\text{J}$	$3.00 \pm 0.24$	$0.77 \pm 0.02$
D-Scan, 31 $\mu\text{J}$	$3.78 \pm 0.30$	$0.76 \pm 0.02$

#### 4. Conclusions

We have extended the formalism of the D-Scan, a method with a simple experimental implementation that delivers quick numerical results, to calculate the pulses superposition at the  $\rho_{\max}$  location, allowing the quantification of incubation effects. To that purpose, we defined a mathematical superposition for the D-Scan, and found an analytical expression for it. We applied the method to a common optical material, and demonstrated that the values obtained are in agreement with the ones given by the traditional method and by the literature, for more than three orders of magnitude. This convergence also confirmed our hypotheses that the superposition  $N$  at a certain position is given by the sum of the intensity of many pulses displaced from this locus, and it is equivalent to the one of the traditional method. Moreover, the expression found is general and allows fractionary superposition of pulses, indicating that

incubation effects are a linear sum of the contribution (intensity) of many pulses that are not required to be in the immediate vicinity of the ablated region.

Additionally, the method introduced is easier to perform and more precise than the traditional one since it requires only a continuous movement of the sample across the beamwaist and a single dimensional measurement to determine the ablation threshold of the sample, in contrast to the traditional one in which many parameters have to be known and be kept under control. Also, the experiment can be done in a few seconds, being less sensitive laser instabilities (pointing, energy), and provides smaller uncertainties than the ones obtained with the traditional method, although a smaller number of measurements is needed.

Furthermore, since laser machining is done in a moving sample, the determination of the ablation threshold by multiple pulses by the D-Scan method reproduces this condition more accurately than the traditional, static, method, especially when machining deep cavities. Consequently, the morphology of the D-Scan etching is the same as the one done by the machining, and better suited to determine the material processing parameters.

As a final remark, the values shown on Table 1 are a consequence of the incubation model [17] used for the fit. If another model, such as the exponential one [15], were used, these values could have been somewhat different. The discussion of the most adequate model to describe the incubation behavior, although of importance for the comprehension of the incubation physical mechanisms, is outside the scope of the present work. The objective of our work was to demonstrate that the D-Scan method allows the calculation of the ablation threshold fluence for the superposition of any number of pulses, yielding the same results as the traditional method, as can be clearly seen by the good data agreement on Fig. 5.

#### **Acknowledgments**

The authors would like to thank FAPESP, SAE and CNPq for financial support.